Biomacromolecules

pubs.acs.org/Biomac

Article

Microphase Separation of Resilin-like and Elastin-like Diblock Copolypeptides in Concentrated Solutions

Luis A. Navarro,[‖] Justin J. Ryan,[‖] Michael Dzuricky, Michael Gradzielski, Ashutosh Chilkoti, and Stefan Zauscher*

Cite This: *Biomacromolecules* 2021, 22, 3827−3838

Read Online

ACCESS | Metrics & More | Article Recommendations | Supporting Information

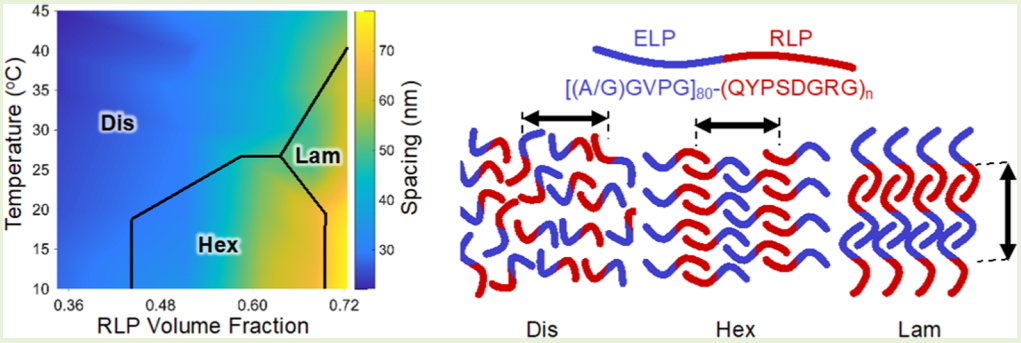

ABSTRACT: Diblock copolymers are valued for their ability to form thin films with nanoscale features that typically reflect those of their microphase-separated structures in concentrated solution. Here, we show that such self-assembled structures can be easily formed with diblock copolymers composed of thermally responsive polypeptides, such as resilin-like polypeptides (RLP) and elastin-like polypeptides (ELP), by exploiting the inverse temperature transition behavior of ELPs in aqueous media. Specifically, we examine the self-assembly of a series of RLP-*b*-ELP diblock copolypeptides in concentrated aqueous solution (30 and 50 wt %) by small-angle X-ray scattering (SAXS). By systematically varying RLP block length and temperature (10−45 °C), we observed microphase separation into hexagonally packed cylinders and lamellae. By analyzing the observed order−order transitions (OOT) and order−disorder transitions (ODT), we determined that self-assembly in this system is primarily driven by polymer−solvent interactions. While these thermally responsive polymers showed clear ODTs and OOTs at certain temperatures, temperature only had a weak effect on the spacing of the resulting nanostructures. In contrast, we found that nanostructure spacing was far more sensitive to RLP block length. Finally, we used atomic force microscopy (AFM) to demonstrate that spin casting RLP-*b*-ELP diblock copolypeptides also produce nanostructured thin films with spacings that correlate with those in concentrated solution.

INTRODUCTION

Many synthetic block copolymers can microphase-separate and form periodic structures with nanoscale features in solution and on surfaces.[1−3] Such microphase-separated nanostructures find application in memory storage,[4,5] as templates for nanocomposites,[2] as metal−organic semiconductor capacitors,[6] in photovoltaics,[7] and as biological scaffolds.[8] While research efforts have primarily focused on studying and harnessing the microphase separation of synthetic block copolymers, the microphase separation of block copolypeptides at high solution concentrations and on surfaces has not yet been explored. Assemblies generated by microphase separation of block copolypeptides can generate three-dimensional nanostructures that could be useful for a broad range of applications, including heterogeneous catalysis,[9] biosensing,[10] drug delivery,[11] and biofuel cells.[12] Nanostructured thin films of block copolypeptides could be exploited to enhance active site accessibility and facilitate the transport of reactants and products, in applications ranging from cell culture substrates to scaffolds to guide tissue regeneration.[12−14] Block copolypeptides have some intrinsic advantages over synthetic block copolymers because they can be produced recombinantly with perfect sequence control and monodispersity and can be fused to other proteins at the gene level.[15] Their synthesis by recombinant expression of a synthetic gene in cells can leverage the cellular infrastructure that already exists to produce, for example, recombinant protein drugs at a large scale.

Received: May 25, 2021
Revised: July 16, 2021
Published: August 13, 2021

https://doi.org/10.1021/acs.biomac.1c00672
Biomacromolecules 2021, 22, 3827−3838

Scheme 1. Structures of the Block Copolypeptides Used in This Study[a]

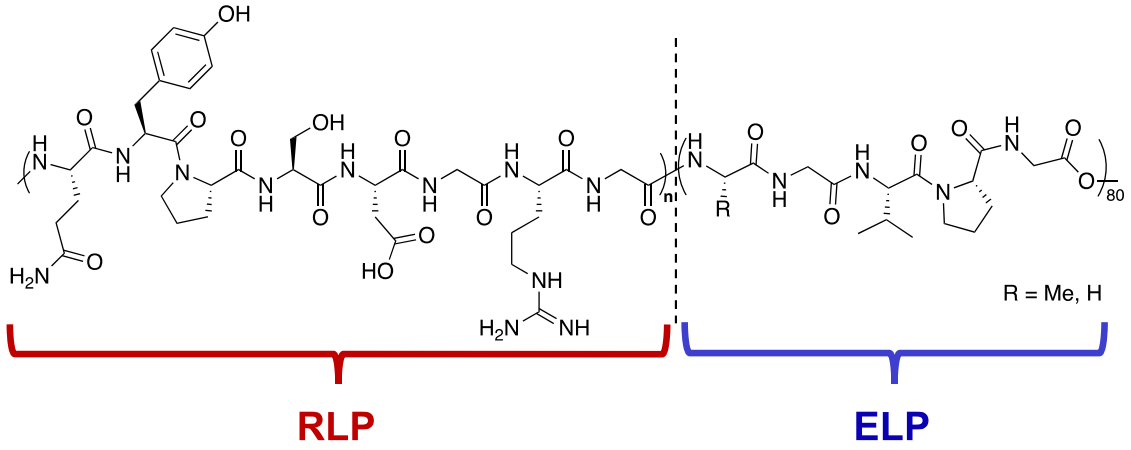

[a]They consist of a resilin-like polypeptide (RLP) block with block lengths that vary from 20 to 100 octapeptide repeat units and an elastin-like polypeptide (ELP) block with 80 pentapeptide repeat units. These diblock copolypeptides have the amino acid sequence G-$(QYPSDGRG)_n$-$[(A/G)GVPG]_{80}$-Y.

Thermally responsive polypeptides excel at self-assembly because the genetically encoded amino acid sequence controls peptide−water interactions, which change dramatically over a narrow temperature range. Elastin-like polypeptides (ELPs) are a well-studied class of thermally responsive polypeptides that exhibit inverse transition phase behavior, often called lower critical solution temperature (LCST) phase behavior.[16] ELPs are artificial intrinsically disordered proteins (IDPs) with the repeat sequence $(VPGXG)_n$, where the inverse temperature transition of the ELP varies between 0 and 100 °C depending on the identity of the guest residue and concentration.[17] Another class of intrinsically disordered proteins are resilin-like polypeptides (RLPs), which are artificial proteins inspired by peptide motifs found in resilin. RLPs were recently found to also exhibit temperature-dependent phase behavior, often called upper critical solution temperature (UCST) behavior.[18] Because ELPs and RLPs lack secondary structure, their conformational behavior mimics that of synthetic polymers in solution. While the inverse transition behavior of ELPs is well understood,[17,19,20] the UCST behavior of RLPs is not as thoroughly documented due to its more recent discovery.[18] ELPs, RLPs, and their diblock copolypeptides have been used to successfully drive self-assembly in solution at low concentrations.[18,21] The useful properties of ELPs and RLPs led us to examine the self-assembly of their block copolymers at high solution concentrations (Scheme 1 and Table 1).

Table 1. Molecular Weights of the Block Copolypeptides Employed in this Study

Polymer	RLP M_n (kDa)	ELP M_n (kDa)	RLP coacervate water content[a]
RLP_{20}-*b*-ELP_{80}	17.2	30.0	62.3%
RLP_{40}-*b*-ELP_{80}	34.4	30.0	53.6%
RLP_{60}-*b*-ELP_{80}	51.7	30.0	50.7%
RLP_{80}-*b*-ELP_{80}	68.9	30.0	50.5%
RLP_{100}-*b*-ELP_{80}	86.1	30.0	ND

[a]Water content is the mass fraction of water in a coacervate of an RLP homopolymer of the same molecular weight.

Block copolymer self-assembly is commonly exploited to create nanostructured thin films. Such films are produced by deposition approaches, most commonly spin coating and subsequent solvent vapor annealing.[22−24] The structure of the resulting thin films appears during deposition[25−27] and is controlled by the block length and the interaction parameters of the different components.[28] The dependence on deposition parameters leads us to hypothesize that the structures observed in thin films likely originate from nanostructures that formed in solution as they were concentrated during spin coating. This motivated us to explore the formation of ordered structures in concentrated polypeptide copolymer solutions and their connection to the structures observed in thin films. In preliminary studies, we observed that RLP-*b*-ELP copolymers formed highly ordered structures in both thin films and concentrated solutions. This included ordered nanostructures typically observed for block copolymer systems, such as lamellae (Lam) and cylinders.

To the best of our knowledge, the microphase separation of thermally responsive polypeptide block copolymers at high solution concentrations is still unexplored. While dual-responsive diblock copolymers have been studied extensively, research has primarily focused on synthetic or hybrid diblock copolymers.[29] Our work on RLP-*b*-ELP is one of the first studies to use solely genetically engineered biomacromolecules, which opens the door to various applications in biosensing, biomedicine, and catalysis. Furthermore, these so-called "schizophrenic" diblock copolymers were primarily studied in dilute solution, frequently focusing on how conditions lead to micelle formation and affect micelle size.[30−34] Prior work from the Chilkoti group on RLP-*b*-ELPs and ELP-*b*-ELPs focused on self-assembly behavior in dilute solution, where micelles were observed.[21,35,36] Our study specifically focuses on concentrated solutions of RLP-*b*-ELPs which produce highly ordered, microphase-separated structures such as lamellae and cylinders. Furthermore, we explicitly compare the ordered structures of block copolypeptides that form in concentrated solutions to those arising in their thin films. As such, RLP-*b*-ELPs provide a unique system to understand the conditions that lead to highly ordered thin films with engineered biopolymers.

https://doi.org/10.1021/acs.biomac.1c00672
Biomacromolecules 2021, 22, 3827−3838

We systematically tested the effects of temperature and RLP molecular weight (block length) on the self-assembly of thermally responsive diblock copolypeptides in concentrated aqueous solution. Specifically, to determine the conditions that cause RLP-*b*-ELP to form different ordered nanostructures, we performed small-angle X-ray scattering (SAXS) on a homologous series of these block copolypeptides over a broad temperature range relevant to handling biologicals (10−45 °C). Furthermore, we studied how temperature, concentration, and polymer composition affect the dimensions of the resulting nanostructures (disordered, cylinders, and lamellae). Our results provide new insights into the role of polymer−solvent interactions in the self-assembly of ordered structures produced by intrinsically disordered proteins at high concentrations. Finally, we examine RLP-*b*-ELP thin films by atomic force microscopy (AFM) and compare the resulting nanostructures on surfaces to those observed in concentrated solution. We find that annealing the thin films at high relative humidity yields precisely defined nanostructures in the thin films that are also present in concentrated solution. We posit that the lack of specific interactions of our polypeptides allows our findings to be applied to a broad range of intrinsically disordered block copolypeptides.

EXPERIMENTAL SECTION

Materials. pET24+ vectors were purchased from Novagen (Madison, WI). gBlock fragments were purchased from Integrated DNA Technologies (Coralville, IA). Ligation enzymes, restriction enzymes, and DNA ladders were purchased from New England BioLabs (Ipswich, MA). BL21 (DE3) chemically competent *Escherichia coli* cells were purchased from Bioline (Taunton, MA). All *E. coli* cultures were grown in Terrific Broth (TB) media purchased from VWR International (Radnor, PA). Kanamycin sulfate was purchased from EMD Millipore (Billerica, MA). Protein expression was induced with isopropyl β-D-1-thiogalactopyranoside (IPTG) from Gold Biotechnology (St. Louis, MO). All salts were purchased from Sigma-Aldrich (St. Louis, MO). 1× Phosphate-buffered saline (PBS) tablets (10 mM phosphate buffer, 140 mM NaCl, 3 mM KCl, pH 7.4 at 25 °C) were purchased from EMD Millipore (Billerica, MA). DNA extraction kits and DNA gel purification kits were purchased from Qiagen, Inc. (Germantown, MD). Whatman Anotop sterile syringe filters (0.02 μm) were purchased from GE Healthcare Life Sciences (Pittsburgh, PA).

Block Copolypeptide Synthesis. All block copolypeptide genes were synthesized from synthetic oligomers using recursive directional ligation by plasmid reconstruction. The block copolypeptides have the form G-$(QYPSDGRG)_n$-$[(A/G)GVPG]_{80}$-Y where the RLP chain length is given by n = 20, 40, 60, 80, or 100 (Table 1). A guest residue of A/G indicates in the ELP block that the guest residue alternates between A and G from one pentapeptide to the next, resulting in a 50/50 ratio between A and G.

Expression and Purification of Block Copolypeptides. Each block copolypeptide was expressed in BL21(DE3) *E. coli* using a previously published hyperexpression protocol, which relies on the leakiness of the T7 promoter.[37] Cultures (50 mL) were grown overnight and used to inoculate 1 L flasks of TB supplemented with 45 μg/mL kanamycin. The flasks were then incubated at 37 °C for 24 h and 190 rpm. Each construct was purified using the previously described inverse transition cycling method.[38,39] Briefly, the cell suspension was centrifuged at 3000 rpm for 10 min at 4 °C, the cell pellet was then resuspended in PBS and then lysed by sonication on ice for 3 min (10 s on, 40 s off) (Misonix S-4000; Farmingdale, NY). Polyethyleneimine (PEI) 0.7% w/v was added to the lysate to precipitate nucleic acid contaminants. The supernatant was then subjected to multiple rounds of inverse transition cycling as follows. The solution was kept on ice, and 3 M NaCl was added to isothermally trigger the phase transition of the ELP. The coacervate was then centrifuged for 10 min at 14000*g* and 20 °C, the supernatant was decanted and discarded, and the pellet was resuspended in phosphate buffer. The suspension was cooled to 4 °C and then centrifuged for 10 min at 14000*g* and 4 °C to remove any insoluble contaminants. Solutions of RLP-*b*-ELP were prepared in Milli-Q water at concentrations of 30 and 50 wt % at 10 °C.

RLP Coacervate Water Content Measurement. A 20 wt % solution of each RLP homopolymer (20, 40, 60, and 80 repeat units) in DI water was heated to 75 °C and periodically vortexed briefly. After about 2 h, the mixtures were either homogeneous or fully dispersible suspensions, depending on the molecular weight of the RLP. The mixtures were allowed to cool to room temperature, and centrifuged at 2000 rcf for 2 min, yielding a clear, brown-amber coacervate and clear, colorless supernatant. The supernatant was carefully removed by a pipette before measuring the wet mass of the coacervate. The amber brown-coacervate was lyophilized for 4 days before measuring its dry mass (white-brown brittle solid). The water content was derived from the ratio of wet and dry mass of coacervate (Table 1).

Small-Angle X-ray Scattering (SAXS). Solutions of RLP-*b*-ELP were prepared in Milli-Q water at concentrations of 30 and 50 wt % at 10 °C by repetitive centrifugation to hydrate the samples. Solution morphologies were measured via small-angle X-ray scattering (SAXS), conducted at Duke University's Shared Materials and Instrumentation Facility (SMIF) using a pinhole collimated SAXSLAB Ganesha instrument. Viscous solutions were placed in sealed Kapton cells and measured at concentrations of 30 and 50 wt % in deionized (Milli-Q) water at temperatures between 10 and 45 °C in increments of 5 °C. The instrument was equipped with a Cu Kα X-ray source, with a characteristic wavelength (λ) of 0.154 nm, and a sample-to-detector distance of 1.08 m. Scattered X-rays were collected on a two-dimensional (2D) Pilatus 300k detector and azimuthally integrated to yield one-dimensional (1D) intensity versus q scattering profiles, where q ($=(4\pi/\lambda)\sin\theta$) represents the scattering vector and θ is half the scattering angle. Scattering profiles were then produced by subtracting the intensity of a blank water sample taken at the same temperature to remove the background. SAXS data were analyzed by four main steps: (1) preliminary assignment of Bragg peaks, (2) identification of the phase based on the Bragg peaks, (3) fitting a full lamellar paracrystal model when applicable, and (4) identifying missing peaks. Data were analyzed using MATLAB R2019a with the Curve Fitting Toolbox (v3.5.11) and SasView (v3.1.0) with a lamellar paracrystal model.[40] For full details on SAXS analysis, see the Supporting Information.

Thin-Film Fabrication. Thin films of polypeptide were deposited on freshly cleaved mica sheets (Ted Pella) using a KW-4A Spin Coater (MicroNano Tools) from a 1 wt % solution in deionized (Milli-Q) water at room temperature. A two-stage deposition procedure was performed by pipetting 70 μL of solution onto the mica substrate and spinning at 500 rpm for 5 s to fully cover the substrate with solution. This was followed by spinning at 3000 rpm for 60 s to ensure full evaporation of solvent. Samples were then allowed to dry overnight at ambient conditions followed by vacuum drying for 24 h at ambient temperature to remove any weakly absorbed water and then characterized without further modification.

Additionally, each polypeptide was further subjected to vapor annealing by enclosing the vacuum-dried substrates in a sealed container with deionized water for 24 h at room temperature, followed by vacuum drying for 24 h and the subsequently characterized. For this procedure, film thicknesses were typically 22 ± 4 nm, measured by spectroscopic ellipsometry (RLP_{80}-*b*-ELP_{80} on silicon).[41]

Atomic Force Microscopy (AFM). Thin-film morphologies of the polypeptides on mica were characterized via AFM using a multimode AFM (Bruker) in tapping mode in air with silicon cantilevers (k_F = 40 N/m, f_{res} = 300 kHz, R_{tip} < 10 nm, Bruker). AFM images were processed using Bruker NanoScope Analysis to plane fit, flatten, and export the images. Exported images were then analyzed with ImageJ (v2.1.0/1.53c) with Fiji. Images were converted to 16-bit color, scaled, converted to 2D Fourier transforms, and adjusted with

https://doi.org/10.1021/acs.biomac.1c00672
Biomacromolecules 2021, 22, 3827−3838

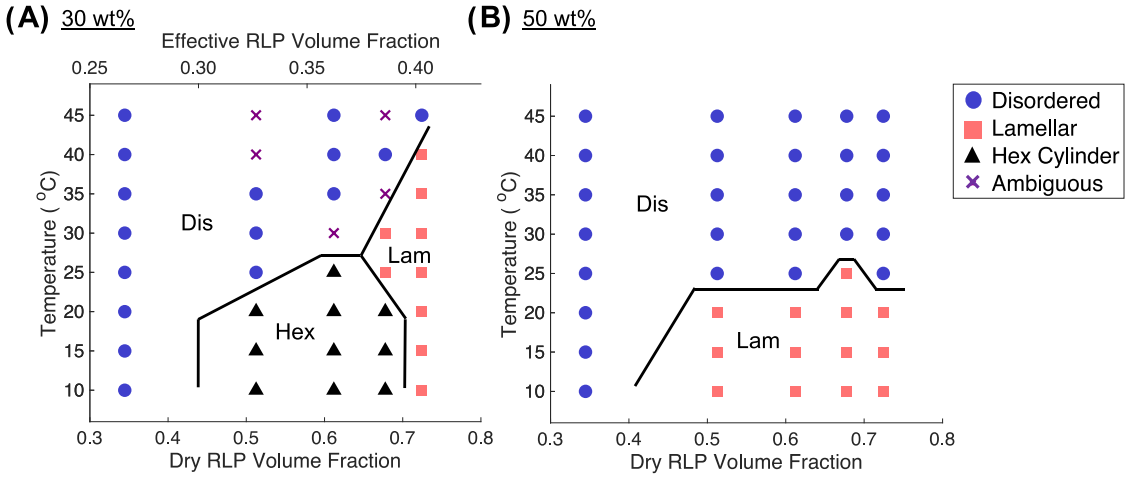

Figure 1. Phase diagram for RLP_n-*b*-ELP_{80} (n = 20, 40, 60, 80, and 100) at (A) 30 wt % and (B) 50 wt % concentration in aqueous solution. Phases are labeled as disordered (Dis, blue solid circle), alternating lamellar (Lam, red solid square), hexagonally packed cylindrical (Hex, black solid triangle), or unknown (X) phases based on SAXS data. Polymer composition is shown as the RLP volume fraction of the dry copolymer (lower x-axis) and as an approximate volume fraction of hydrated RLP of the 30 wt % mixture (upper x-axis, see Effective RLP Volume Fraction in the Supporting Information). Under these solution conditions, the RLP is insoluble below 50 °C while the ELP exhibits an inverse temperature transition around 20−25 °C (see the Role of Polymer−Solvent Interactions section).

brightness/contrast to highlight the ring at the center of the Fourier transformed image. The Radial Profile Extended plugin was used to determine the center of the ring (as determined by the mode of the normalized intensity).

RESULTS AND DISCUSSION

Experimental Design Choices. Our goal was to investigate the effects of temperature, composition, and concentration on the self-assembly of RLP-*b*-ELP block copolypeptides in concentrated aqueous solution. Specifically, we chose to use an ELP and RLP for each block because these polymers are thermally responsive. This allows us to use changes in temperature to tune the polymer−solvent interaction for each block. Additionally, the sequence and chain length of these block copolymers can be perfectly controlled through recombinant synthesis. To elucidate the effects of composition on self-assembly, we expressed a homologous series of RLP-*b*-ELP diblock copolypeptides with constant ELP block length, but variable RLP block length (Scheme 1). We examined these polymers with SAXS to determine the size and morphology of ordered phases. Specifically, we studied the self-assembly of these polymers at high solution concentrations (30 and 50 wt %) to mimic conditions during thin-film formation upon solvent evaporation. Finally, we focused on a temperature range (10−45 °C) most relevant for applications of protein polymers, accepting that the RLP block is well below its transition temperature.

Morphology of Block Copolypeptides in Concentrated Solution. We observed microphase separation in the block copolypeptides at both 30 and 50 wt % over a wide range of block sizes and temperatures (Figure 1). The main structures we observed were disordered (Dis), hexagonally packed cylinders (Hex), and lamellae (Lam). Structures were assigned by examining the pattern of Bragg peaks in the block copolymers' scattering profiles (Figure 2). Specifically, lamellar structures show characteristic peaks at q^*, $2q^*$, $3q^*$, and $4q^*$, while Hex structures show peaks at q^*, $\sqrt{3}\,q^*$, $2q^*$, and $\sqrt{7}\,q^*$.[42] However, some samples with hexagonally packed structures were missing peaks at $\sqrt{3}\,q^*$ and/or $3q^*$ (Figure S22). The

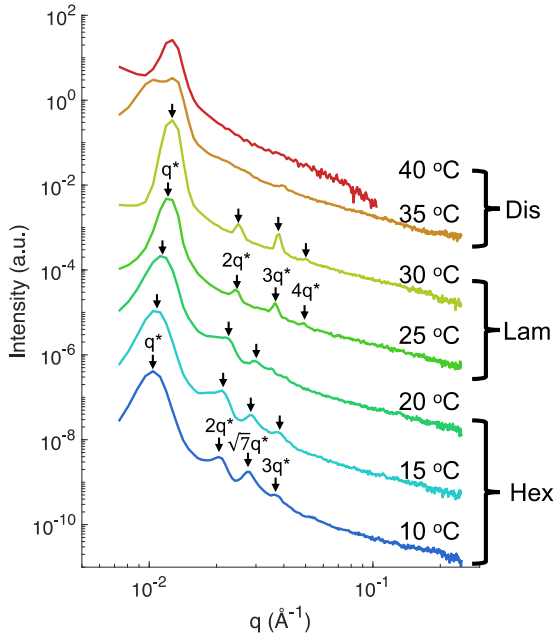

Figure 2. Scattering profiles of RLP_{80}-*b*-ELP_{80} from 10 to 40 °C at 30 wt % concentration measured by SAXS. Representative Bragg peaks are marked (↓) based on their relation to the principal peak for lamellar and hexagonal cylindrical phases. Scattering profiles are arbitrarily offset for clarity.

suppression of these peaks has been previously observed in other copolymer systems,[43,44] and is typically attributed to the destructive interference of the cylinder's form factor with a structure factor peak at specific values of the cylinder radius. In our case, the hexagonal cylinder radius we predict for RLP_{60}-*b*-ELP_{80} at 10−15 °C at 30 wt % leads to a form factor with minima at 0.024 and 0.036 Å^{-1}. These minima match the missing Bragg peaks that are expected at 0.022 and 0.038 Å^{-1}.

Figure S17 shows the presence of a principal scattering peak that persists even with the disappearance of higher-order Bragg peaks that are characteristic of ordered structures. In the disordered phase, the principal peak persists to higher

https://doi.org/10.1021/acs.biomac.1c00672
Biomacromolecules 2021, 22, 3827−3838

temperatures with increasing RLP block length or concentration. With increasing temperature, the height of this principal peak decreases as its width increases, indicating a gradual loss of structure that produces this peak. This peak persists to higher temperatures with increasing RLP block length or concentration. It is unlikely that these peaks arise from polymer−polymer correlation because ELP and RLP have very similar scattering length densities, 1.23×10^{-5} and 1.36×10^{-5} Å^{-2}, respectively. In combination with the fact that these polymers have small radii (~5 nm in dilute solution),[21] the clearly defined principal peaks suggest the presence of disordered structures as opposed to free chains.[45] The lack of features in the scattering profiles of the disordered systems make assigning a specific structure challenging in the absence of additional information. However, at high RLP composition, we know that these disordered structures are produced by heating either lamellae or cylinders above the order−disorder transitions (ODT), which stems from the collapse of the ELP block (see the Role of Polymer−Solvent Interactions section). Therefore, by a curvature argument, the disordered structure is likely a bicontinuous phase at high RLP fraction lacking long-range order, whereas we expect disordered micelles with RLP-rich cores at low RLP fractions. However, SAXS alone is ineffective to distinguish between these structures.

In general, when varying the RLP block size or temperature, the scattering behavior of the block copolypeptides at a given concentration showed only small differences in the high q range (>0.06 Å^{-1}) (Figures S19 and S20). As the high q range relates to the molecular structure of the polymers, this observation indicates that the polymers have an internal structure that is consistent across different temperatures and molar masses at a given concentration. In contrast, we observed larger differences in scattering behavior at high q when comparing the profiles from 30 and 50 wt % solutions (Figure S21), which suggests that the molecular-level structure is sensitive to concentration.

Role of Polymer−Solvent Interactions. The primary interactions to consider in the RLP-*b*-ELP system are the polymer−polymer and polymer−solvent interactions. As order−disorder transition (ODT) temperatures are higher at the lower concentration (Figure 1), ordered phases form more readily with a greater fraction of solvent. This implies that the polymer−solvent interactions dominate over the polymer−polymer interaction because added solvent facilitates the phase separation. While these polymer−solvent interactions depend on composition, our choice of thermally responsive polymers causes this interaction to have a strong temperature dependence. Therefore, we examined the role of temperature on the polymer−solvent interactions in the context of these microphase-separated structures.

For this discussion, it is helpful to first understand each block's transition temperature and how it is expected to change at high concentration in the presence of the other block. The RLPs have transition temperatures in the range of 30−45 °C at around 1 wt % concentration, below which they aggregate (Figure S5). Extrapolating dilute solution data for RLP_{60} or RLP_{100} to 30 wt % yields a transition temperature of approximately 50 or 68 °C, respectively. As all our experiments were carried out below the transition temperature of the RLPs, we expect the RLP blocks to collapse and expel water. In contrast, the ELP homopolymer exhibits an inverse temperature transition in dilute aqueous solution at around 50 °C.[17,20] We expect the transition temperature of the ELP block to be lowered by the combination of (i) high concentration of ELP, (ii) the linkage of the polypeptides in a block copolymer, and (iii) the high RLP fraction. It is known that the transition temperature of ELP homopolymers decreases with increasing ELP concentration.[20] Second, RLP-*b*-ELPs already exhibit a lower transition temperature than the ELP homopolymer (38−45 °C) in dilute solution.[21] Third, we can better understand how the high RLP fraction influences the ELP block's transition temperature at high solution concentrations by comparing ELP to poly(*N*-isopropylacrylamide) (PNIPAM)—a synthetic polymer with LCST behavior in aqueous media.[46] PNIPAM's transition temperature decreases substantially in the presence of high concentrations of poly(ethylene oxide) (PEO).[47] This behavior is attributed to a change in the activity of water, similar to that of salting-out ions.[47] Thus, we expect the high fraction of RLP to further reduce the transition temperature of the ELP through a similar competition with water.

With this background, we can better interpret the effect of temperature on the observed order−disorder transitions that appear in our phase diagrams. In general, the transition temperatures of the homopolymers discussed above do not appear in our RLP-*b*-ELP phase diagrams (Figure 1). The water−ELP interaction changes at the ELP's transition temperature, which should be significantly lowered as a result of the high concentrations of both ELP and RLP in solution (ranging from 7.7 to 32 wt % and from 11 to 37 wt %, respectively). At 50 wt %, there is a single main boundary for the order−disorder transition around 20−25 °C. At a similar temperature range, hexagonally packed cylinders at 30 wt % also undergo an order−disorder transition. Thus, it is likely that these transitions are associated with the inverse temperature transition behavior of the ELP, which reflects a dramatic change in the interaction between water and the ELP.[48] This assignment is corroborated by the shrinking of lamellar structures due to the collapse of the ELP in RLP_{100}-*b*-ELP_{80} at 30 wt % in the range of 20−25 °C (see the Microphase-Separated Structures section). However, the order−disorder transition for lamellar phases at 30 wt % occurs at substantially higher temperatures (30−45 °C), which suggests that the lamellar structures are stable beyond the ELP's transition temperature, and only disintegrates at a much higher temperature.

In addition to revealing order−disorder transitions, the scattering data also reveal differences between strong and weak ordering based on the emergence of higher-order peaks.[43] Generally, we observe higher-order scattering peaks at lower temperatures. For example, in the temperature range from 10 to 25 °C, RLP_{60}-*b*-ELP_{80} produces hexagonally packed phases at 30 wt %. The scattering profile taken at 25 °C reveals Bragg peaks up to $\sqrt{7}q^*$, whereas the scattering profile at 10 °C reveals a peak even at $\sqrt{16}q^*$ (Figure S23). The solution concentration also affects the emergence of higher-order peaks. For example, for lamellar RLP_{100}-*b*-ELP_{80} at 15 °C, we observe higher-order peaks up to $\sqrt{16}q^*$ at 30 wt %, but only up to $\sqrt{4}q^*$ at 50 wt %. Thus, decreasing temperature and decreasing concentration lead to more elaborate long-range order with larger and better-defined grains. We attribute these trends to changes in the strength of polymer−solvent interactions that affect the ordering of the self-assembled structures. While polymer−polymer interactions are also likely at play, we hypothesize that these interactions are sensitive to

https://doi.org/10.1021/acs.biomac.1c00672
Biomacromolecules 2021, 22, 3827−3838

polymer hydration, and therefore influenced by polymer−solvent interactions. Specifically, lower temperatures increase the solvent quality for the ELP while the RLP remains collapsed, which leads to a stronger solvent selectivity at lower temperatures.

The stronger ordering observed at 30 wt % can be explained by the partitioning of water between the RLP-rich and ELP-rich microphases. We estimated the water content of the collapsed RLP-rich phase by measuring the water content of coacervates of pure RLP homopolymer (Table 1). We can exploit this measurement if we assume that the ELP-rich domains are hydrated and that the collapsed RLP-rich domains mimic the structure of an RLP homopolymer coacervate. In this case, self-assembly should be disrupted when the water content of the RLP coacervate exceeds the water content of the entire mixture because this would lead to the collapsed block being more hydrated than the swollen block. However, this situation is nonsensical at temperatures where water is an ELP-selective solvent. The water content that we observed for each coacervate just barely exceeds 50%, which is consistent with the greater prevalence of disordered phases at 50 wt % than at 30 wt %. This leads us to speculate that the structures formed by RLP-*b*-ELP at 50 wt % are evidence for weak segregation because there is insufficient water content to generate RLP-pure microdomains (cylinders or lamellae) that mimic coacervates of RLP homopolymer, while simultaneously maintaining a disproportionately hydrated ELP-pure microphase.

Furthermore, we found that the RLP_{20} coacervate has a substantially higher water content (62%) than the higher-molecular-weight polymers (50−53%). The phase behavior of RLP_{20} is unique in that it fails to form ordered phases in concentrated solution (this study) and also fails to form micelles in dilute solution.[21] We believe that these observations are connected because the water−polymer interaction is the main driving force for self-assembly in this system. Because shorter RLPs form coacervates with higher water content (Table 1), shorter RLPs will cause a smaller disparity in the water content between the two domains in the block copolypeptides, and thus weaker segregation. This compounds with the generally weaker ability of copolymers to form self-assembled structures if they have lower molecular weight or have a more asymmetric composition.

Because the observed self-assembly behavior is dominated by ELP−water interactions, we expect the hydrophobicity of the ELP's guest residue to profoundly impact the self-assembly of RLP-*b*-ELP copolymers. This concept was explored previously in ELP-*b*-mCherry fusion proteins, where ELPs with higher hydrophobicity or molar mass promoted self-assembly in a highly concentrated solution.[49] By the same reasoning, our findings suggest that ELP sequences can be rationally designed to achieve specific, ordered structures at a desired combination of temperature, concentration, and RLP composition.

Microphase-Separated Structures. The observed phase boundaries of the various ordered structures provide us with further insight into the self-assembly of RLP-*b*-ELP at high concentrations, specifically: (i) the identity of ELP-rich versus RLP-rich domains, (ii) water partitioning between domains, and (iii) the selectivity of the solvent. For our discussion, we will focus on the phase diagram at 30 wt %, because at this concentration, we observed a greater variety of phases than at 50 wt % (Figure 1A).

First, the ordering of phases in the RLP-*b*-ELP block copolypeptides mirrors that of diblock copolymer melts. In these melts, diblock copolymers generally form disordered, cylindrical, then lamellar structures in order of increasingly symmetric comonomer composition.[1] We observe the same ordering of structures in the 30 wt % samples as we increase the RLP fraction in the copolypeptide. From a curvature argument, adding length to the RLP block of the cylinder would only lead to the observed lamellar phase if the cylinders are RLP-rich. Thus, we conclude that the hexagonal phase is composed of RLP-rich cylinders in an ELP-rich continuous domain (matrix).

Second, the polymer compositions that produce ordered phases have a much higher RLP volume fraction than we would expect for a canonical diblock copolymer melt. For example, lamellar phases are only observed above 65% RLP volume fraction, and hexagonally packed cylinders are still observed above 50% RLP volume fraction. A similar phenomenon was observed for polystyrene-*b*-polyisoprene in styrene-selective solvents.[50] This departure from the canonical phase diagram observed for our copolymers likely arises from the difference in the partitioning of water between microdomains. Due to the thermally responsive behaviors of the homopolymers, we expect water to be a selective solvent for the ELP and to preferentially partition into the ELP-rich phase. As a result, the effective volume fraction of hydrated RLP versus hydrated ELP is much less than the volume fraction of the RLP in the dry copolymer. Thus, we reason that the water's selective partitioning into the ELP-rich microdomains causes ordered phases to only appear for asymmetric, RLP-rich diblock copolymers. This also explains the prevalence of lamellar phases at 50 wt %, because the partitioning of water should lead to more symmetric effective volume fractions at which lamellar structures commonly form.

Third, to better understand the nature of the phase boundary, we examined the spacing of lamellar structures formed by RLP_{100}-*b*-ELP_{80} at 30 wt % by fitting them to a lamellar paracrystal model (Figures 3 and 4A). The lamellar

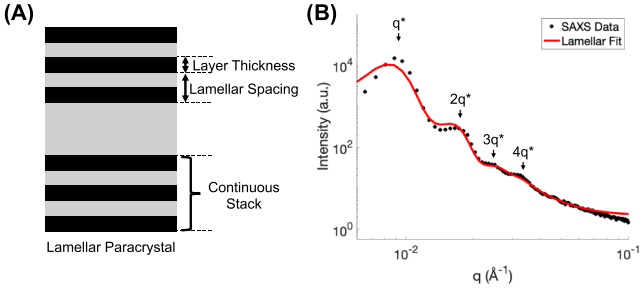

Figure 3. (A) Model for a lamellar paracrystal. (B) Representative fit of a lamellar paracrystal model (red) to SAXS data (black) for RLP_{100}-*b*-ELP_{80} at 30 wt % at 20 °C.

spacing abruptly shrinks between 20 and 25 °C. This temperature range also coincides with the range over which we observe order−order or order−disorder transitions in the $RLP_{40\text{-}80}$-*b*-ELP_{80} copolymer system. We thus attribute the change in lamellar spacing to the collapse of the ELP chains in the continuous domain, defining a clear split in the phase diagram where the collapsed RLP block is accompanied by a hydrated ELP block below 20 °C and both blocks are collapsed above 25 °C. Below 20 °C, water is a highly selective solvent

https://doi.org/10.1021/acs.biomac.1c00672
Biomacromolecules 2021, 22, 3827−3838

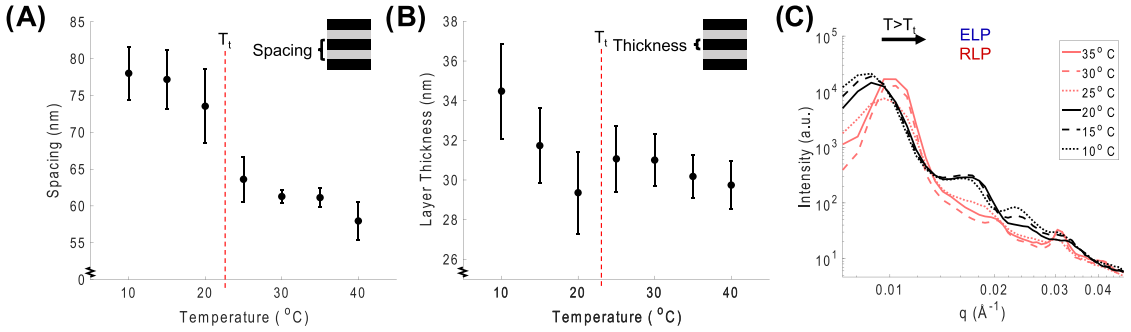

Figure 4. Dimensions of lamellar structures observed for RLP_{100}-*b*-ELP_{80} in 30 wt % aqueous solution. (A) Lamellar spacing and (B) layer thickness as functions of temperature. The transition temperature (T_t) of the ELP is indicated near 22 °C. (C) Scattering curves highlight differences below 22 °C (black) and above 22 °C (red). The insets visually illustrate that lamellar spacing refers to the periodic dimension of the lamella, while layer thickness refers to the width of a single sheet of the RLP-rich domain. Values are obtained from fitting SAXS data to a lamellar paracrystal model (Figure 3).

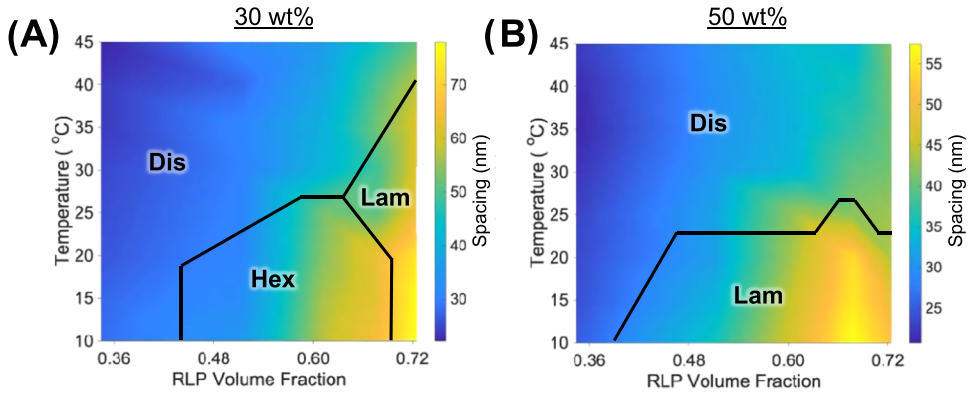

Figure 5. Dimensions of RLP_n-*b*-ELP_{80} nanostructures at various temperatures and RLP compositions at (A) 30 wt % and (B) 50 wt % aqueous solution. The spacings are derived from SAXS data. For disordered (Dis) phases, the spacing is derived from the principal peak ($2\pi/q^*$). For hexagonally packed cylinders (Hex), the spacing corresponds to the distance between the centers of adjacent cylinders ($4\pi/q^*\sqrt{3}$). For lamellae (Lam), the spacing corresponds to the lamellar spacing obtained from fitting to a lamellar paracrystal model.

that gives rise to hexagonally packed phases over a wide range of polymer compositions. In contrast, water becomes a less selective solvent with increasing temperatures, hindering microphase separation as seen by the prevalence of disordered phases. Combined, our observations indicate that the LCST behavior of the ELP block can result in an order−disorder transition ($RLP_{40\text{-}60}$-*b*-ELP_{80}), order−order-transition (RLP_{80}-*b*-ELP_{80}), or solely a conformational change while retaining its lamellar morphology (RLP_{100}-*b*-ELP_{80}).

Controlling Nanostructure Dimensions. In practice, it is useful to control the dimensions of a self-assembled structure to tailor it to a given application. To this end, we examined how temperature, RLP block length (volume fraction), and concentration impact the dimensions of the various nanostructures that form (Figure 5). We observe that the size of the nanostructures becomes larger with decreasing temperature, with increasing RLP volume fraction, and with decreasing polymer concentration. Figure 5 also shows that molecular weight (composition) has the largest effect on nanostructure size, as the larger polymers simply lead to much larger spacings (~2× across samples). In contrast, at a fixed molecular weight, temperature has only a small effect on nanostructure size. The stronger dependence of spacing with molecular weight than with temperature is expected and typical of block polymer systems.

Dimensions of the Lamellar Phases. Here, we discuss the variation in lamellar dimensions with respect to: (i) temperature, (ii) concentration, and (iii) RLP volume fraction. The clearest demonstration of temperature dependence on lamellar dimensions can be seen in RLP_{100}-*b*-ELP_{80} at 30 wt % (Figure 4). We chose to discuss this sample because it uniquely forms lamellar structures across a wide range of temperatures at this concentration. We modeled these structures with a lamellar paracrystal model to determine both the layer thickness and the lamellar spacing (Figure 3). Despite the thermally responsive nature of RLP_{100}-*b*-ELP_{80}, temperature has generally little impact on the dimensions of the nanostructures, except near the ELP's transition temperature, where the ELP−water interaction changes dramatically. A comparison of Figure 4A,B shows that the lamellar spacing decreases significantly at the transition temperature, while the layer thickness has no apparent trend. The combination of a constant layer thickness and changing lamellar spacing leaves some volume of expelled water unaccounted, which we speculate partitions into the regions separating continuous lamellar stacks. Furthermore, we infer that the temperature-insensitive layer corresponds to the RLP-rich domain based on: (1) the composition of the block copolypeptide, (2) the partitioning of water, and (3) the fact that the layer thickness is generally less than half of the lamellar spacing (for further discussion, see the Supporting Information).

As we only tested two concentrations, we have a limited ability to make claims about concentration dependence. Nevertheless, if we assume a power law relationship, as is

https://doi.org/10.1021/acs.biomac.1c00672
Biomacromolecules 2021, 22, 3827−3838

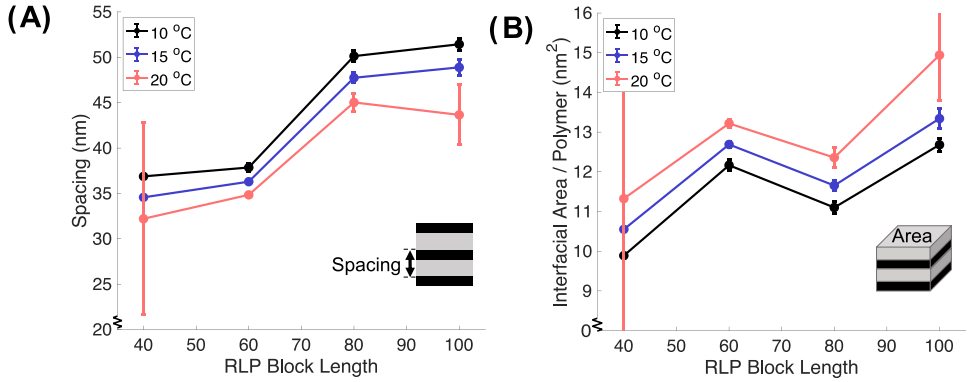

Figure 6. (A) Lamellar spacing and (B) interfacial area per polymer in RLP$_n$-*b*-ELP$_{80}$ at 50 wt % varies with RLP block length (in octapeptides) at different temperatures. Spacings were obtained by fitting a lamellar paracrystal model to SAXS data. Interfacial areas were calculated from spacings (see Extended Discussion in the Supporting Information).

observed for other copolymer systems in the literature (i.e., spacing ~ volume fraction$^{-\beta}$),[51] then for lamellar structures of RLP$_{100}$-*b*-ELP$_{80}$, we obtain exponents of β = 0.91 and 0.82 for lamellar spacing and lamellar thickness, respectively. These exponents are significantly larger than those observed in other systems, e.g., polystyrene-*b*-polyisoprene lamellae in tetradecane showed $\beta \sim 0.2$.[51] However, exponents as high as 1.0 are predicted for systems that feature strongly selective solvents and copolymers with a small mass fraction of the soluble block.[51] Thus, it is reasonable that we observe a strong concentration scaling because our RLP-*b*-ELP system exhibits both of these features.

Finally, we examine the effects of RLP block length on lamellar domain size. Figure 6A shows that the lamellar spacing decreases weakly with increasing temperature (below the ELP's transition temperature) but increases markedly with increasing RLP block length. A particularly large size increase takes place between RLP$_{60}$ and RLP$_{80}$ across all temperatures. While spacing is expected to increase with the molecular weight of the RLP block, the observed trend deviates from the $d \sim MW^{2/3}$ scaling that is typical for block copolymers in the melt.[52−54] This discrepancy is best explained through the scaling of interfacial area per polymer chain (Figure 6B), where larger polymer chains should consume more area within the lamellae. However, the area consumed per polymer chain instead decreases when RLP block length increases from RLP$_{60}$ to RLP$_{80}$. This suggests a change to a more extended conformation of the block copolymer. We speculate that the absence of the canonical $d \sim MW^{2/3}$ scaling stems from the competitive partitioning of water between the ELP-rich and RLP-rich microdomains. As the two blocks compete for solvent at 50 wt %, a longer RLP block not only increases the potential size of the RLP domains, but also affects the distribution of water between the RLP-rich and ELP-rich domains. Thus, we suspect that this competition for solvent causes the conformational change that then leads to the unexpected dependence of lamellar spacing on block length.

Dimensions of Hexagonally Packed Phases. Figure 7 shows that for hexagonally packed cylinders at 30 wt %, higher temperatures led to slightly smaller spacings (larger q^* values). As with the lamellae, the effect of temperature is insubstantial in comparison to the effect of block length, as longer RLP blocks dramatically increase the spacing between cylinders. Because the length of the soluble ELP block is fixed in our system, increasing the length of the insoluble RLP block leads

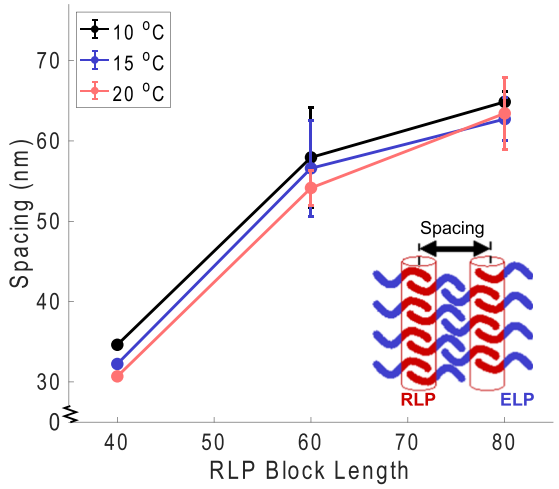

Figure 7. Hexagonal cylinder spacing in RLP$_n$-*b*-ELP$_{80}$ at 30 wt % varies with RLP block length at different temperatures. The spacing was determined from the positions of Bragg peaks present in SAXS data. (Inset) This spacing is shown as a distance between hexagonally packed cylinders.

to a higher polymer density per unit length of the cylinder (Figure S26). However, the increase in spacing of the hexagonally packed phase is larger than the calculated increase in the diameter of each cylinder (Figure S2, see also Extended Discussion in the Supporting Information). Therefore, a longer RLP block leads to both a greater cylinder radius and a larger distance between the cylinders in the ELP-rich domain, which in turn contributes to a larger hexagonal cylinder spacing.

Dimensions of Disordered Phases. We also examined the spacings in the disordered phase (Figure 8). As mentioned above, the disordered phase most likely has an indeterminate transition between micellar and bicontinuous structures when changing from short to long RLP block lengths. While this makes a more detailed analysis of the spacing in these structures challenging, we can still provide a qualitative analysis of the trends in spacing. As with lamellar and cylindrical morphologies, temperature has little impact on polymer dimension in the disordered phase, while block length has a large influence. We attribute the negligible temperature dependence to both blocks being collapsed between 30 and 45 °C. Figure 8 shows that spacing increases with RLP block length, as expected. While the scaling of this relationship appears to be sensitive to concentration at first glance, this

https://doi.org/10.1021/acs.biomac.1c00672
Biomacromolecules 2021, 22, 3827−3838

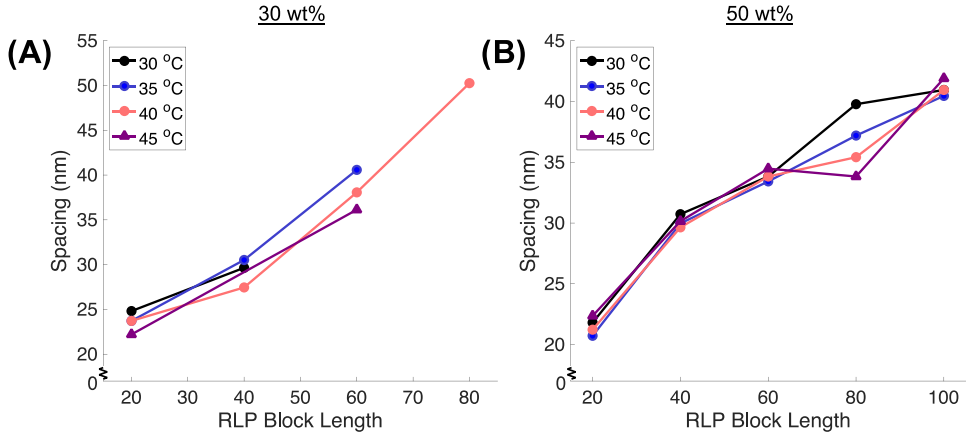

Figure 8. Spacing observed in disordered structures in RLP$_n$-*b*-ELP$_{80}$ varies with RLP block length at different temperatures at (A) 30 wt % and (B) 50 wt %. Spacing was determined from the principal peak in the SAXS scattering profiles.

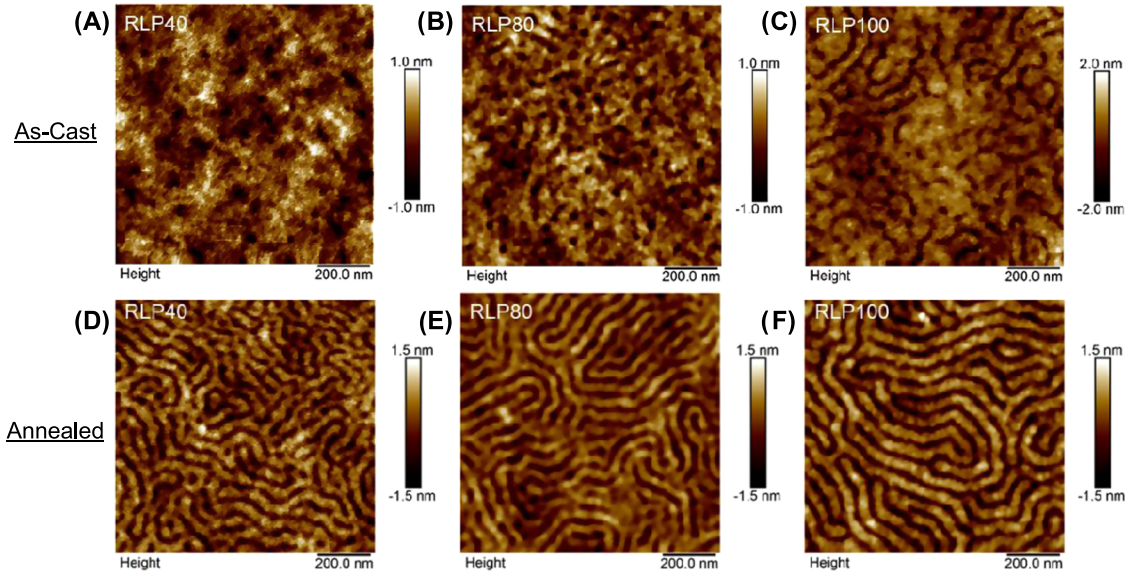

Figure 9. AFM height images of RLP$_n$-*b*-ELP$_{80}$ thin films on mica were captured by tapping mode in air (A–C) before and (D–F) after solvent annealing. Thin films are shown for (A, D) RLP$_{40}$-*b*-ELP$_{80}$, (B, E) RLP$_{80}$-*b*-ELP$_{80}$, and (C, F) RLP$_{100}$-*b*-ELP$_{80}$. A significant refinement in nanostructure was observed for all samples after solvent annealing in a high-humidity environment for 24 h. Lower-magnification images are available in the Supporting Information (Figure S24).

difference is not statistically significant (see Extended Discussion in the Supporting Information). When fit to a power law (spacing ~ (RLP block length)^n), we measured exponents of 0.53 and 0.38 at 30 and 50 wt %, respectively. These scaling exponents are substantially larger than those associated with poor solvent scaling (0.33). This is consistent with the proposed hydration of the RLP block in these structures. Finally, as with the ordered structures, the spacing of the disordered structures also decreases substantially with increasing concentration. This is a natural consequence of the removal of water from the structure.

Block Copolymer Morphology on Surfaces. We investigated the formation of nanostructures in spin-coated thin films of RLP-*b*-ELP by AFM. Figure 9A–C shows that the morphologies of the as-cast films are poorly defined. To remedy this, we annealed the films with solvent vapor, which typically promotes block copolymer thin films to adopt more thermodynamically stable morphologies by enhancing polymer mobility.[23] Indeed, solvent annealing caused RLP$_n$-*b*-ELP$_{80}$ thin films to adopt well-defined cylindrical or lamellar morphologies similar to those observed in concentrated solution (Figure 9D–F). This suggests that spin coating arrests the block copolypeptides in kinetically trapped structures that are far removed from the structurally well-defined morphologies that better represent equilibrium structures.

As the polypeptide concentration gradually increases during the spin coating process, we can compare the spacings that occur in RLP-*b*-ELP thin films with those occurring in solution to better understand how these ordered structures evolve. We discuss the data obtained for RLP$_{100}$-*b*-ELP$_{80}$ as a representative example. By analyzing the 2D Fourier transform of AFM height images of this block copolypeptide, we measured spacings of 80.5 and 56.6 nm for RLP$_{100}$-*b*-ELP$_{80}$ before and after solvent vapor annealing, respectively. The spacing in the as-cast thin films is larger than the spacing observed in a 30 wt % solution by SAXS (80.5 versus 73.5 nm) (Figure S25). Furthermore, the as-cast film morphologies show some features that resemble perpendicularly oriented cylinders that could have originated from cylindrical micelles known to form

https://doi.org/10.1021/acs.biomac.1c00672
Biomacromolecules 2021, 22, 3827–3838

in dilute solution (Figure 9C).[21] This suggests that the as-cast films contain kinetically trapped structures that resemble those found also in dilute solution. Solvent vapor annealing then allowed the copolymer film to relax into highly ordered structures that qualitatively resemble lamellar structures, such as those observed in concentrated solution by SAXS. Additionally, these structures have a spacing of 56.6 nm which lies between the spacings observed at 30 and 50 wt % in solution, i.e., 73.5 and 43.6 nm, respectively. Thus, we propose that annealed RLP_{100}-*b*-ELP_{80} thin films have lamellar structures that resemble those observed in concentrated solution.

CONCLUSIONS

In this study, we demonstrate that thermoresponsive block copolypeptides (RLP-*b*-ELP) can form a range of self-assembled structures in concentrated solution, including lamellae, hexagonally packed cylinders, and disordered structures. By using blocks that are individually thermally responsive in aqueous solution, the block copolypeptides form ordered phases whose emergence is driven by temperature-dependent interactions with water, which acts as a strongly block-selective solvent for this block copolypeptide system. Self-assembly of the RLP-*b*-ELPs into ordered structures occurs more readily below 25 °C, i.e., temperatures at which the RLP block is collapsed and the ELP block is swollen. Strong polymer−solvent interactions cause hexagonally packed cylinders to form over a large range of block copolymer compositions at 30 wt %. Additionally, higher temperatures cause the ELP block to collapse, which favors the formation of disordered phases and decreases the dimensions of ordered phases. The general preference for water to partition into the ELP phase naturally causes the RLP block to occupy a much smaller effective volume fraction in solution than its volume fraction in the dry copolymer. As a result, the emergence of ordered structures requires the polymer's dry composition to be primarily RLP (>50% by volume). When correcting for the water content in each domain, the phase behavior of these copolypeptides resembles the canonical phase behavior of diblock copolymer melts with respect to the relative location of disordered, hexagonal, and lamellar phases. The observed phase diagram is most consistent with phases that contain RLP-rich cylinders in a continuous, ELP-rich domain. While we did not exploit the UCST behavior of RLPs in this study, as all experiments were conducted below their transition temperature. For future work, manipulating the RLP sequence to express a reasonably low transition temperature would be interesting to potentially invert the microphases, as seen in schizophrenic micelles.

The dimensions of the nanostructures depend on temperature, concentration, and composition. Despite their narrow range of accessible temperatures, temperature can be used to effectively control these self-assembled structures through sharp transitions at which the polymer−solvent interaction changes dramatically. Higher temperatures reduce the size of the copolypeptide structures by decreasing the solvent quality. As these transition temperatures are primarily dependent on the amino acid sequence, we believe that sequence control is the most effective way to control the temperature ranges in which specific ordered structures appear. The most effective way to control the sizes of the nanostructures was through molecular weight and concentration. While spacing increases intuitively with higher-molecular-weight polymers, we did not observe the canonical power law behaviors for block copolymers reported in the literature for lamellae. The trend has a step at a critical RLP block length at which there is a conformational change to more extended polymer chains. While the origin of this conformational change is unknown, we speculate that it is tied to the partitioning of water in this system which is expected to depend on RLP molecular weight. Finally, the use of a strongly selective solvent caused nanostructures to shrink dramatically with increasing polymer concentration.

The RLP-*b*-ELP nanostructures observed in concentrated solution also form in spin-coated thin films on surfaces. The emergence of such precisely defined nanostructures on surfaces after solvent annealing is exciting because it is the first and most critical step to fabricate highly ordered, biomolecular nanostructures over macroscopically large areas. The understanding of how different conditions affect RLP-*b*-ELP microphase separation in bulk solution, should allow one to tailor these surface structures to specific applications. Finally, because the formation of microphase-separated RLP-*b*-ELP structures at high concentration was primarily driven by polymer−solvent interactions, it is likely that similar ordered nanostructures arise with different amphiphilic proteins, even in the absence of specific interactions or secondary structures.

ASSOCIATED CONTENT

Supporting Information

The Supporting Information is available free of charge at https://pubs.acs.org/doi/10.1021/acs.biomac.1c00672.

Additional discussion, experimental details, protein characterization, SAXS data (plots and tables), AFM images, and plots of microstructure dimensions (PDF)

AUTHOR INFORMATION

Corresponding Author

Stefan Zauscher − *Department of Mechanical Engineering & Materials Science, Duke University, Durham, North Carolina 27708, United States; Department of Biomedical Engineering, Duke University, Durham, North Carolina 27708, United States;* orcid.org/0000-0002-2290-7178; Email: zauscher@duke.edu

Authors

Luis A. Navarro − *Department of Mechanical Engineering & Materials Science, Duke University, Durham, North Carolina 27708, United States;* orcid.org/0000-0002-7536-308X

Justin J. Ryan − *Department of Mechanical Engineering & Materials Science, Duke University, Durham, North Carolina 27708, United States*

Michael Dzuricky − *Department of Biomedical Engineering, Duke University, Durham, North Carolina 27708, United States;* orcid.org/0000-0002-1775-2132

Michael Gradzielski − *Institut of Chemistry, Technische Universität Berlin, 10623 Berlin, Germany;* orcid.org/0000-0002-7262-7115

Ashutosh Chilkoti − *Department of Biomedical Engineering, Duke University, Durham, North Carolina 27708, United States;* orcid.org/0000-0002-1569-2228

Complete contact information is available at: https://pubs.acs.org/10.1021/acs.biomac.1c00672

Author Contributions

[‖]L.A.N. and J.J.R. contributed equally to this work.

Funding

This work was funded by the NSF through DMREF-1729671 and MRSEC DMR-11-21107. Additionally, this work was supported by the NIH: R01GM061232, R01EB000188, and R01EB007205. The authors acknowledge the Duke University Shared Materials and Instrumentation Facility (SMIF) for maintaining the SAXS instrument used in this work. L.A.N. holds a Graduate Diversity Enrichment Program Award from the Burroughs Wellcome Fund.

Notes

The authors declare no competing financial interest.

■ ACKNOWLEDGMENTS

Special thanks go to Prof. Timothy Lodge for helpful discussions on the topic of block copolymer microphase separation.

■ REFERENCES

(1) Leibler, L. Theory of Microphase Separation in Block Copolymers. *Macromolecules* **1980**, *13*, 1602−1617.
(2) Darling, S. B. Directing the self-assembly of block copolymers. *Prog. Polym. Sci.* **2007**, *32*, 1152−1204.
(3) Stoykovich, M. P.; Nealey, P. F. Block copolymers and conventional lithography. *Mater. Today* **2006**, *9*, 20−29.
(4) Thurn-Albrecht, T.; Schotter, J.; Kastle, G. A.; Emley, N.; Shibauchi, T.; Krusin-Elbaum, L.; Guarini, K.; Black, C. T.; Tuominen, M. T.; Russell, T. P. Ultrahigh-density nanowire arrays grown in self-assembled diblock copolymer templates. *Science* **2000**, *290*, 2126−2129.
(5) Kim, H. C.; Park, S. M.; Hinsberg, W. D. Block copolymer based nanostructures: materials, processes, and applications to electronics. *Chem. Rev.* **2010**, *110*, 146−177.
(6) Black, C. T.; Guarini, K. W.; Milkove, K. R.; Baker, S. M.; Russell, T. P.; Tuominen, M. T. Integration of self-assembled diblock copolymers for semiconductor capacitor fabrication. *Appl. Phys. Lett.* **2001**, *79*, 409−411.
(7) Darling, S. B. Block copolymers for photovoltaics. *Energy Environ. Sci.* **2009**, *2*, 1266−1273.
(8) Liu, J.; Zhang, Q.; Remsen, E. E.; Wooley, K. L. Nanostructured materials designed for cell binding and transduction. *Biomacromolecules* **2001**, *2*, 362−368.
(9) Hartmann, M. Ordered Mesoporous Materials for Bioadsorption and Biocatalysis. *Chem. Mater.* **2005**, *17*, 4577−4593.
(10) Endo, T.; Kerman, K.; Nagatani, N.; Hiepa, H. M.; Kim, D. K.; Yonezawa, Y.; Nakano, K.; Tamiya, E. Multiple label-free detection of antigen-antibody reaction using localized surface plasmon resonance-based core-shell structured nanoparticle layer nanochip. *Anal. Chem.* **2006**, *78*, 6465−6475.
(11) Jacob, J.; Haponiuk, J. T.; Thomas, S.; Gopi, S. Biopolymer based nanomaterials in drug delivery systems: A review. *Mater. Today Chem.* **2018**, *9*, 43−55.
(12) Minteer, S. D.; Liaw, B. Y.; Cooney, M. J. Enzyme-based biofuel cells. *Curr. Opin. Biotechnol.* **2007**, *18*, 228−234.
(13) Olsen, B. D. Self-Assembly of Globular-Protein-Containing Block Copolymers. *Macromol. Chem. Phys.* **2013**, *214*, 1659−1668.
(14) Ho, M.-H.; Kuo, P.-Y.; Hsieh, H.-J.; Hsien, T.-Y.; Hou, L.-T.; Lai, J.-Y.; Wang, D.-M. Preparation of porous scaffolds by using freeze-extraction and freeze-gelation methods. *Biomaterials* **2004**, *25*, 129−138.
(15) Li, L.; Tong, Z.; Jia, X.; Kiick, K. L. Resilin-Like Polypeptide Hydrogels Engineered for Versatile Biological Functions. *Soft Matter* **2013**, *9*, 665−673.
(16) Varanko, A. K.; Su, J. C.; Chilkoti, A. Elastin-Like Polypeptides for Biomedical Applications. *Annu. Rev. Biomed. Eng.* **2020**, *22*, 343−369.
(17) Urry, D. W. Physical chemistry of biological free energy transduction as demonstrated by elastic protein-based polymers. *J. Phys. Chem. B* **1997**, *101*, 11007−11028.
(18) Li, L.; Luo, T.; Kiick, K. L. Temperature-triggered phase separation of a hydrophilic resilin-like polypeptide. *Macromol. Rapid Commun.* **2015**, *36*, 90−95.
(19) McDaniel, J. R.; Radford, D. C.; Chilkoti, A. A unified model for de novo design of elastin-like polypeptides with tunable inverse transition temperatures. *Biomacromolecules* **2013**, *14*, 2866−2872.
(20) Meyer, D. E.; Chilkoti, A. Quantification of the effects of chain length and concentration on the thermal behavior of elastin-like polypeptides. *Biomacromolecules* **2004**, *5*, 846−851.
(21) Weitzhandler, I.; Dzuricky, M.; Hoffmann, I.; Garcia Quiroz, F.; Gradzielski, M.; Chilkoti, A. Micellar Self-Assembly of Recombinant Resilin-/Elastin-Like Block Copolypeptides. *Biomacromolecules* **2017**, *18*, 2419−2426.
(22) Wadley, M. L.; Hsieh, I. F.; Cavicchi, K. A.; Cheng, S. Z. D. Solvent Dependence of the Morphology of Spin-Coated Thin Films of Polydimethylsiloxane-Rich Polystyrene-block-Polydimethylsiloxane Copolymers. *Macromolecules* **2012**, *45*, 5538−5545.
(23) Jung, F. A.; Berezkin, A. V.; Tejsner, T. B.; Posselt, D.; Smilgies, D. M.; Papadakis, C. M. Solvent Vapor Annealing of a Diblock Copolymer Thin Film with a Nonselective and a Selective Solvent: Importance of Pathway for the Morphological Changes. *Macromol. Rapid Commun.* **2020**, *41*, No. 2000150.
(24) Sinturel, C.; Vayer, M.; Morris, M.; Hillmyer, M. A. Solvent Vapor Annealing of Block Polymer Thin Films. *Macromolecules* **2013**, *46*, 5399−5415.
(25) Fustin, C.-A.; Huang, H.; Hoogenboom, R.; Wiesbrock, F.; Jonas, A. M.; Schubert, U. S.; Gohy, J. F. Evaporation induced micellization of poly(2-oxazoline) multiblock copolymers on surfaces. *Soft Matter* **2007**, *3*, 79−82.
(26) Huang, W.; Luo, C.; Zhang, J.; Han, Y. Formation of ordered microphase-separated pattern during spin coating of ABC triblock copolymer. *J. Chem. Phys.* **2007**, *126*, No. 104901.
(27) Kim, G.; Libera, M. Morphological Development in Solvent-Cast Polystyrene−Polybutadiene−Polystyrene (SBS) Triblock Copolymer Thin Films. *Macromolecules* **1998**, *31*, 2569−2577.
(28) Elbs, H.; Drummer, C.; Abetz, V.; Krausch, G. Thin Film Morphologies of ABC Triblock Copolymers Prepared from Solution. *Macromolecules* **2002**, *35*, 5570−5577.
(29) Papadakis, C. M.; Muller-Buschbaum, P.; Laschewsky, A. Switch It Inside-Out: "Schizophrenic" Behavior of All Thermoresponsive UCST-LCST Diblock Copolymers. *Langmuir* **2019**, *35*, 9660−9676.
(30) Weaver, J. V. M.; Armes, S. P.; Bütün, V. Synthesis and aqueous solution properties of a well-defined thermo-responsive schizophrenic diblock copolymer. *Chem. Commun.* **2002**, *18*, 2122−2123.
(31) Wang, D.; Wu, T.; Wan, X.; Wang, X.; Liu, S. Purely salt-responsive micelle formation and inversion based on a novel schizophrenic sulfobetaine block copolymer: structure and kinetics of micellization. *Langmuir* **2007**, *23*, 11866−11874.
(32) Sun, H.; Chen, X.; Han, X.; Liu, H. Dual Thermoresponsive Aggregation of Schizophrenic PDMAEMA-b-PSBMA Copolymer with an Unrepeatable pH Response and a Recycled CO2/N2 Response. *Langmuir* **2017**, *33*, 2646−2654.
(33) Vishnevetskaya, N. S.; Hildebrand, V.; Niebuur, B.-J.; Grillo, I.; Filippov, S. K.; Laschewsky, A.; Müller-Buschbaum, P.; Papadakis, C. M. "Schizophrenic" Micelles from Doubly Thermoresponsive Polysulfobetaine-b-poly(N-isopropylmethacrylamide) Diblock Copolymers. *Macromolecules* **2017**, *50*, 3985−3999.
(34) Vishnevetskaya, N. S.; Hildebrand, V.; Niebuur, B.-J.; Grillo, I.; Filippov, S. K.; Laschewsky, A.; Müller-Buschbaum, P.; Papadakis, C. M. Aggregation Behavior of Doubly Thermoresponsive Polysulfobetaine-b-poly(N-isopropylacrylamide) Diblock Copolymers. *Macromolecules* **2016**, *49*, 6655−6668.

https://doi.org/10.1021/acs.biomac.1c00672
Biomacromolecules 2021, 22, 3827−3838

(35) Hassouneh, W. Understanding Elastin-Like Polypeptide Block Copolymer Self-assembly Behavior. Dissertation, Duke University, 2013.
(36) Hassouneh, W.; Zhulina, E. B.; Chilkoti, A.; Rubinstein, M. Elastin-like Polypeptide Diblock Copolymers Self-Assemble into Weak Micelles. *Macromolecules* **2015**, *48*, 4183−4195.
(37) Guda, C.; Zhang, X.; McPherson, D. T.; Xu, J.; Cherry, J. H.; Urry, D. W.; Daniell, H. Hyper expression of an environmentally friendly synthetic polymer gene. *Biotechnol. Lett.* **1995**, *17*, 745−750.
(38) Trabbic-Carlson, K.; Liu, L.; Kim, B.; Chilkoti, A. Expression and purification of recombinant proteins from *Escherichia coli*: Comparison of an elastin-like polypeptide fusion with an oligohistidine fusion. *Protein Sci.* **2004**, *13*, 3274−3284.
(39) Meyer, D. E.; Chilkoti, A. Purification of recombinant proteins by fusion with thermally-responsive polypeptides. *Nat. Biotechnol.* **1999**, *17*, 1112−1115.
(40) Bergström, M.; Pedersen, J. S.; Schurtenberger, P.; Egelhaaf, S. U. Small-Angle Neutron Scattering (SANS) Study of Vesicles and Lamellar Sheets Formed from Mixtures of an Anionic and a Cationic Surfactant. *J. Phys. Chem. B* **1999**, *103*, 9888−9897.
(41) Gao, Y. Microphase Separation of Stimulus-Responsive Block-co-Polypeptides on Surfaces. Master's Thesis, Duke University, 2018.
(42) Hamley, I. W.; Castelletto, V. Small-angle scattering of block copolymers. *Prog. Polym. Sci.* **2004**, *29*, 909−948.
(43) Lam, C. N.; Olsen, B. D. Phase transitions in concentrated solution self-assembly of globular protein−polymer block copolymers. *Soft Matter* **2013**, *9*, 2393−2402.
(44) Hajduk, D. A.; Gruner, S. M.; Rangarajan, P.; Register, R. A.; Fetters, L. J.; Honeker, C.; Albalak, R. J.; Thomas, E. L. Observation of a reversible thermotropic order-order transition in a diblock copolymer. *Macromolecules* **1994**, *27*, 490−501.
(45) Park, M. J.; Char, K.; Bang, J.; Lodge, T. P. Order−Disorder Transition and Critical Micelle Temperature in Concentrated Block Copolymer Solutions. *Macromolecules* **2005**, *38*, 2449−2459.
(46) Schild, H. G.; Tirrell, D. A. Interaction of poly(N-isopropylacrylamide) with sodium n-alkyl sulfates in aqueous solution. *Langmuir* **1991**, *7*, 665−671.
(47) Maeda, Y.; Taniguchi, N.; Ikeda, I. Changes in the Hydration State of a Block Copolymer of Poly(N-isopropylacrylamide) and Poly(ethylene oxide) on Thermosensitive Micellization in Water. *Macromol. Rapid Commun.* **2001**, *22*, 1390−1393.
(48) Cho, Y.; Zhang, Y.; Christensen, T.; Sagle, L. B.; Chilkoti, A.; Cremer, P. S. Effects of Hofmeister anions on the phase transition temperature of elastin-like polypeptides. *J. Phys. Chem. B* **2008**, *112*, 13765−13771.
(49) Qin, G.; Perez, P. M.; Mills, C. E.; Olsen, B. D. Effect of ELP Sequence and Fusion Protein Design on Concentrated Solution Self-Assembly. *Biomacromolecules* **2016**, *17*, 928−934.
(50) Lodge, T. P.; Pudil, B.; Hanley, K. J. The full phase behavior for block copolymers in solvents of varying selectivity. *Macromolecules* **2002**, *35*, 4707−4717.
(51) Lai, C. J.; Russel, W. B.; Register, R. A. Scaling of domain spacing in concentrated solutions of block copolymers in selective solvents. *Macromolecules* **2002**, *35*, 4044−4049.
(52) Helfand, E.; Wasserman, Z. R. Block Copolymer Theory. 4. Narrow Interphase Approximation. *Macromolecules* **1976**, *9*, 879−888.
(53) Matsushita, Y.; Mori, K.; Saguchi, R.; Nakao, Y.; Noda, I.; Nagasawa, M. Molecular weight dependence of lamellar domain spacing of diblock copolymers in bulk. *Macromolecules* **1990**, *23*, 4313−4316.
(54) Kawasaki, K.; Ohta, T.; Kohrogui, M. Equilibrium morphology of block copolymer melts. 2. *Macromolecules* **1988**, *21*, 2972−2980.

https://doi.org/10.1021/acs.biomac.1c00672
Biomacromolecules 2021, 22, 3827−3838